DFT study of mechanical, optoelectronic, and thermoelectric characteristics of double perovskites Li_2CuTiZ_6 (Z = Cl, Br, I) for energy harvesting technology

N. A. Noor[a,*], K. Abid[b], I. M. Moussa[c], S. Mumtaz[d]
[a]*Department of Physics, Riphah International University, Lahore Campus, Lahore*
[b]*Institute of Electrical, Electronics and Computer Engineering University of the Punjab*
[c]*Department of Botany and Microbiology, College of Science, King Saud University, P.O. Box 2455, Riyadh, 11451, Saudi Arabia;*
[d]*Electrical and Biological Physics, Kwangwoon University, Seoul, 01897, South Korea*

Recent studies have produced stable inorganic perovskites that contain no lead, replacing lead-containing perovskites' risky and unstable properties. The present investigation thoroughly examined the electrical behavior, elastic characteristics, optical features, and transport properties of Li_2CuTlZ_6 (Z = Cl, Br, I) halides in order to discover potential applications. The Wien2k code was utilized to apply density functional theory (DFT) in order to clarify these physical properties. Using the generalized gradient approximation (PBEsol-GGA), we determined structural parameters through the energy optimization procedure that corresponded with the available data. Additionally, elastic parameters as well as formation energies ranging between -2.33 to -1.39 eV were used to validate cubic durability for the two halides. Moreover, the modified Becke-Johnson (mBJ) potential successfully provided precise direct bandgap values for all halides. According to this study, the shift in anions from Cl to Br is responsible for the reduction in band gap within the infrared spectrum. Our computed optical parameter findings show that $Li_2CuTlCl_6$ and $Li_2CuTlBr_6$ halides demonstrate excellent optoelectronic efficiency with low reflection, strong optical absorption, and conductivity. The investigation clarifies that the temperature-dependent character of the materials electrical transport properties is due to their very small bandgap. These materials may find use in thermoelectric applications, as evidenced by the almost unity of the obtained figure of merit, which points to their semiconducting behaviour.

(Received January 11, 2024; Accepted April 5, 2024)

Keywords: First principle investigation, Double perovskites, Elastic constant, Direct bandgap, Absorption co-efficient, Figure of merit

1. Introduction

Growing energy needs lead to a greater reliance on fossil fuels, which increases pollution and accelerates global warming. Silicon solar cells may be a good option for the energy crisis. Nonetheless, there are a lot of difficulties because of the cells reported low power conversion efficiency and the complicated production process. Photovoltaic materials that are simple, affordable, and environmentally benign are used to produce electricity. According to the report (2022), Perovskite solar cells have shown a remarkable rise in efficiency, rising around thirty two percent[1-6]. Halogen based DPs, with the composition UVY_3, are the subject of much research in optoelectronic applications. In this article monovalent cations are denoted by U, divalent cations by V, while halides by Y. Nonetheless, the commercial use of lead-containing solar cells is associated with worries of toxicity and instability [7, 8]. Challenges to human health and the ecosystem are presented by lead and other heavy-density metallic substances. Consequently, it is essential to remove these components from solar energy systems. [9, 10]. Because of this, scientists are replacing lead (Pb) in photovoltaic (PV) devices with non-toxic materials. For the

* Corresponding author: naveedcssp@gmail.com
https://doi.org/10.15251/JOR.2024.202.209

lead-free element to function as efficiently as lead-based devices, it has to fulfill a set of requirements. The substitutes must exhibit advantageous optoelectronic characteristics, be reasonably priced, and be easily recyclable [11, 12].

Because of their low electron/hole masses, changeable bandgap, as well as optical absorption coefficients, double perovskites are considered efficient and eco-friendly. Researchers are interested in double halide perovskites based on Sb and Bi because of their effective optoelectronic characteristics. With lower bandgaps and remarkable stability, DPs Cs_2NBiCl_6 (N = K, Rb, Cs) and Cs_2NaBY_6 (B = Sb, Bi; Y = Cl, Br, I) showed promising optoelectronic applications[13, 14]. Numerous papers have detailed the performance of Cs_2CuNCl_6 (N = Sb, Bi) and related perovskites [15-22]. Over the past few years, thermoelectric technology has attracted much interest. The formula $ZT = (S^2\ \sigma\ T)/(K_e+K_l)$ can be used to determine the thermoelectric efficiency of solids. The Seebeck coefficients are represented by S in this equation, electrical conductivity is represented by σ, absolute temperature is indicated by T, lattice thermal conductance is represented as k_l, and k_e represents e^- conducting behavior due to heat [23, 24]. When a material's estimated ZT value is 1, its thermoelectric performance is efficient [25]. Both elevated PF estimates and low k_e contribute to the materials high ZT value. Although there is not enough experimental research about these double halide perovskites' thermoelectric efficiency, curiosity about their thermoelectric behavior is rapidly increasing. ZT values near unity have been found in a number of hybrid and halide perovskites that have been theoretically investigated, such as Cs_2AgBiX_6 (X = Cl, Br) [26] and Rb_2InBiX_6 (X = Cl, Br) [27]. These results imply that understudy materials have direct energy bandgaps that are tunable and have potential uses in energy manufacturing.

Because of all the benefits halides DPs have above their lead-containing counterparts, they have garnered a lot of interest in the area of materials technology and science [28, 29]. It is important to consider the advantages of these lead-free DP halides in relation to the selected materials, such as the DP Li_2CuTlZ_6 (Z = Cl, Br, I). As lead is hazardous, perovskite materials containing lead may pose health and environmental risks. Lead-free DP, such as Li_2CuTlZ_6 (Z = Cl, Br, I), alleviates these concerns and is safer and more environmentally acceptable for optoelectronic and thermoelectric applications.

2. Computational methods

We applied the DFT-oriented FPLAPW+lo technique, to examine the electronic, optical, and thermal characteristics of Li_2CuTlX_6 (X= Cl, Br, I) DPs [30]. PBEsol-GGA approximation is being employed for assessing mechanical characteristics [31]. Additionally, mBJ potential is utilized to optimize the convergence energy and electrical structure, producing more accurate energy gap measurements [32]. The electrical system's solution is reflected spherically harmonized in the muffin tin sphere but behaves as a plane wave in the interstitial region. Utilizing l = 10, Gmax = 16, the Gaussian parameter, the muffin radius and wave vector product in the reciprocal lattice, and $K_{max}\times R_{MT} = 8$, the basic characteristics are enhanced. 2000 k-points are used to choose the k-mesh in a 12 ×12 × 12 order so that the system's energy output is continuous. The precision of calculated results is limited by convergence threshold requirements. The BoltzTraP algorithm, which is based on Boltzmann theory, was used to calculate the transport characteristics [33].

3. Results and discussion

3.1. Structural and mechanical characteristics

As indicated in Ref. 34, a number of variables, such as the Born stability criterion and formation energy, are employed for assessing the material's durability. Anions and cations also impact the material's band structure and structural stability. Halide double perovskites have the band shape determined by X, Y(I) as well as $Y'(III)$ basis using formula $A_2Y(I)Y'(III)X_6$ having family Fm-3m (225) with cubic structure (depicted in Fig. 1). The mechanical aspects of halogen-based DPs were revealed and the framework viability was confirmed using the Birch-Murnaghan

equation of state. Optimization of double perovskites Li_2CuTlZ_6 (Z = Cl, Br, I) being displayed (Figure 2). Table 1 illustrates the ground state lattice constants of under-analysis DPs.

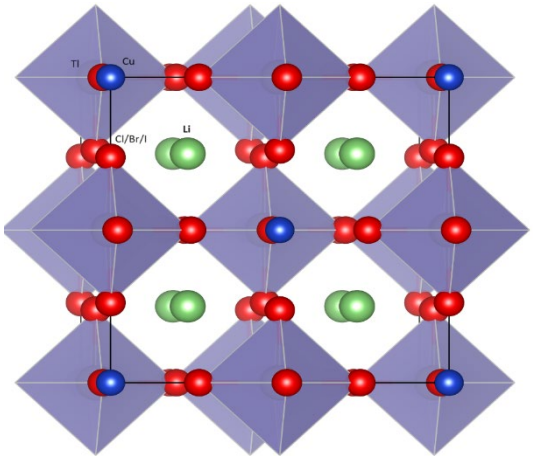

Fig. 1. Structural representation of double perovskites Li_2CuTlX_6 (X = Cl, Br, I) halides.

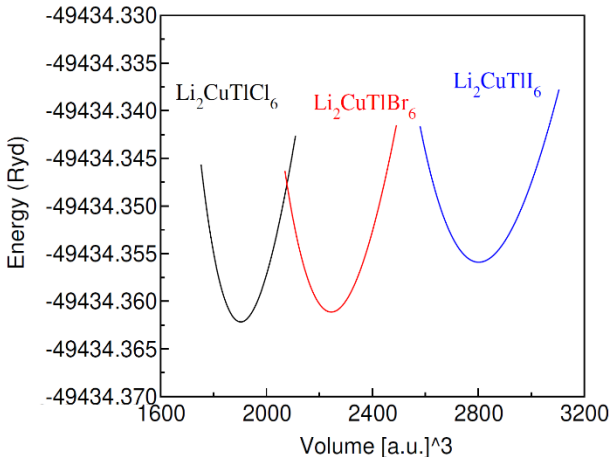

Fig. 2. Optimal graph of investigated double perovskites Li_2CuTlX_6 (X = Cl, Br, I) halides.

By calculating E_{Form} [11, 35], structural stability is further verified. The E_{Form} is calculated using the equation that follows:

$$E_{Form} = (E_{tot} - \sum N_i E_{i-bulk}) / \sum N_i \quad (1)$$

Table 1 contained the estimated figures of E_{Form} for Li_2CuTlZ_6 (Z = Cl, Br, I). The structural stability of the material is shown by the negative sign of E_{Form}. Given the negative calculated value, both materials are regarded as structurally stable.

Using cubic elastic packages, the mechanical characteristics, as well as elastic constants of Li2CuTlZ6 (Z = Cl, Br, I), are investigated. By introducing a little strain into the equilibrium cubic structure, we are able to calculate the SOECs. It may be concluded that the cubic phase is more stable if its energy is less than the distorted structure's. Such condition is also satisfied through Born stability criteria as $C_{11} - C_{12} > 0, C_{11} > 0, C_{44} > 0, C_{11} + 2C_{12} > 0, C_{12} < B < C_{11}$[36]. Elasticity along the unit cells axis is defined by the longitudinal elastic constant, C_{11}, and elasticity in form is defined by the shear elastic constants, C_{12} and C_{44}[37]. Table 1 contains the computed

elastic parameters and all are +ve. The anisotropy of the material is calculated using the Second-Order Elastic Constants (SOECs); a divergence from unity indicates anisotropy [38-40].

Table 1. Estimated figures of lattice constant a_o(Å), bulk modulus B_o(GPa), formation energy (ΔH_f), and elastic parameters of Li_2CuTlZ_6 (Z = Cl, Br, I) halides.

Parameters	$Li_2CuTlCl_6$	$Li_2CuTlBr_6$	Li_2CuTlI_6
	PBEsol-GGA	PBEsol-GGA	PBEsol-GGA
a_o(Å)	10.41	11.00	11.84
B_o (*GPa*)	33.17	26.70	20.05
ΔH_f (eV)	-2.33	-2.07	-1.91
C_{11}	43.12	40.30	33.88
C_{12}	29.92	18.32	11.99
C_{44}	12.02	4.13	1.21
B	34.32	25.58	19.12
G	9.53	6.16	3.43
Y	26.11	17.12	9.73
B/G	3.59	4.15	5.55
υ	0.37	0.38	0.41
A	0.84	0.37	0.11

According to the calculated anisotropy values, both materials show a high degree of anisotropy. As previously mentioned, the SOECs played a vital role in the computation of Poisson's ratio (υ). Furthermore, the calculation of the mean of the modulus of elasticity was done by the Reuss-Voigt-Hill approach. For both materials, the computed value of C_{11} is significantly more than the shear elastic constants (C_{11}−C_{12}). At the same time, the structural durability is significant in terms of volume strain as B>G. These values ((B/G) and υ) meet the parameters' defined requirements [41, 42], suggesting that DPs Li_2CuTlZ_6 (Z = Cl, Br, I) become ductile, while it is clear that ionic bonding predominates.

3.2. Optoelectronic properties

The material's electrical characteristics, such as electron dispersion across the band structure, dictate its potential applications [43]. To reveal the electrical characteristics of Li_2CuTlZ_6 (Z = Cl, Br, I), DFT was utilized. The band structure of double perovskites Li_2CuTlZ_6 (Z = Cl, Br, I) is illustrated using the mBJ technique (see Fig. 3).

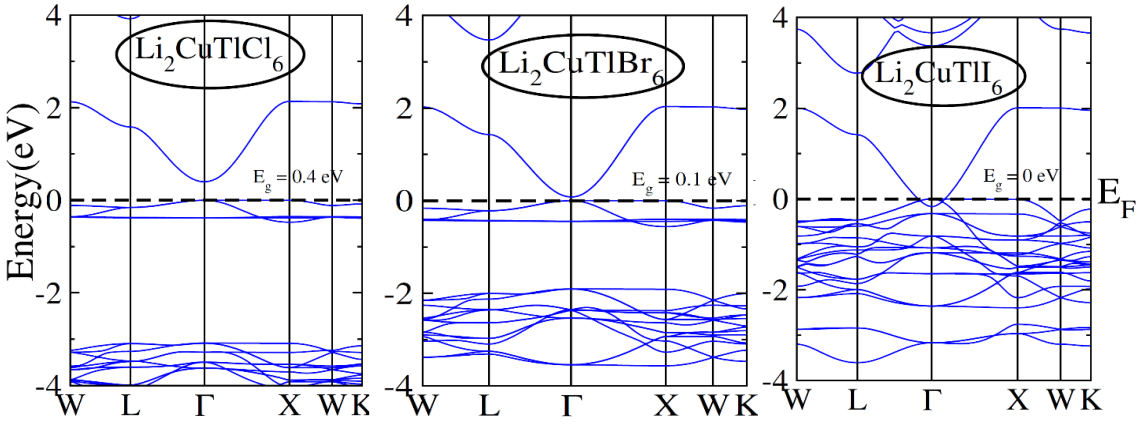

Fig. 3. Calculations of electronic band structure for the $Li_2CuTlCl_6$, $Li_2CuTlBr_6$, and Li_2CuTlI_6 halides.

The semiconducting nature of double perovskites is shown due to the existence of empty regions at E_F. A direct bandgap is seen when the CB minimum and VB maximum meet on the same symmetric locations for DPs $Li_2CuTlCl_6$ (E_g = 0.4 eV) and $Li_2CuTlBr_6$ (E_g = 0.1 eV). Meanwhile, the CB minima and VB maxima overlap for Li2CuTlI6, which has a zero bandgap value. The density of states (DOS) explains the relative representation of the energy states, conduction state, and valence state. The mBJ potential was used to calculate the TDOS and PDOS in Li_2CuTlZ_6, as depicted in Figure 4. These configurations show the VB levels, which include the 3p state of Cl, the 4p state of Br, the 2s state of Li as well as the 6p state of Tl.

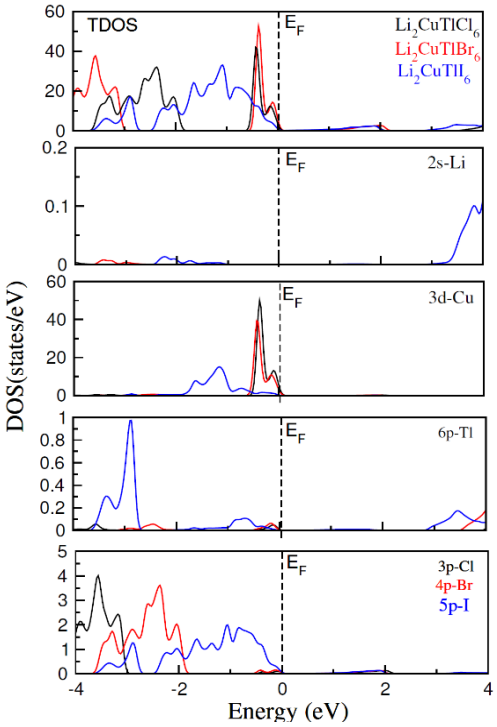

Fig. 4. Estimated TDOS along through PDOS $Li_2CuTlCl_6$, $Li_2CuTlBr_6$ as well as Li_2CuTlI_6..

Interestingly, these topologies are mostly controlled by the halides p-orbitals around the E_F. Meanwhile, electrons derived within the Cl/Br-p orbitals form the upper valence band (VB). The Tl-6p - Li-2s states have no ability to accurately capture the electronic properties of the double perovskites under study because they are not found close to a Fermi level. Under the Fermi level, unoccupied Tl-6p states are hosted in the conduction band (CB), whereas Li-2s contribute to the valence band (VB) in DPs Li_2CuTlZ_6. Since unpaired electrons have been found in the component atoms of the materials under analysis, structural optimization is responsible for forming non-magnetic behavior in these materials. The double perovskites (DPs) under examination exhibit semiconducting behavior and a small bandgap, which renders such attractive options for thermoelectric as well as optoelectronic uses in devices.

3.3. Optical characteristics

The optical characteristics of a material are analyzed via dielectric parameters ($\varepsilon(\omega) = \varepsilon_1(\omega) + i\varepsilon_2(\omega)$), as mentioned by the citations [44-46]. At this point, both components were represented by symbols $\varepsilon_1(\omega)$ and $\varepsilon_2(\omega)$, correspondingly. One of the most important characteristics of materials in electromagnetics is their dielectric constant. It has substantial physical meaning and measures how a substance reacts to an applied electric field. Elevated dielectric constants are frequently observed in materials with high dielectric strength. This characteristic affects light velocity, transmission, and reflection at material surfaces. It has become a very important factor in designing optical equipment.

According to these sources, the dielectric constant's real and imaginary components are required to calculate a number of aforementioned main features, like an index of refraction n(ω) reflectivity R(ω) as well as absorption parameters [47, 48]. Figure 5(a-f) illustrates the observed optical characteristics of the DPs $Li_2CuTlCl_6$ and $Li_2CuTlBr_6$ (0-8 eV). Here the compound's polarization behaviour in response to a given em rays corresponds to $\varepsilon_1(\omega)$, whereas $\varepsilon_2(\omega)$ indicates the compound's radiation absorbing behaviour. For DPs $Li_2CuTlCl_6$ and $Li_2CuTlBr_6$, it is noted that the static $\varepsilon_1(0)$ ratios were 3.6 and 4.4, respectively. The computed figures are in agreement with Penn's model, as explained by the following expression: $\varepsilon_1(0) \approx 1 + (\frac{\hbar\omega_p}{E_g})^2$ [49, 50].

Furthermore, in the visible region, the principal peak of $\varepsilon_1(\omega)$ is around 0.6 eV for $Li_2CuTlCl_6$ and 0.2 eV for $Li_2CuTlBr_6$. After that, $\varepsilon_1(\omega)$ constantly drops to 1.8 eV and then quickly drops. Details on the light absorption properties of these substances are shown in Figure 5(a). The electrical bandgap values and the computed optical bandgap for the DPs $Li_2CuTlCl_6$ and $Li_2CuTlBr_6$ using $\varepsilon_2(\omega)$ consent. The difference in the speeds at which the VB, as well as CB transition, leads to variations in peak intensities. For $Li_2CuTlCl_6$, the highest absorption is 2.3 at 1.8 eV, while for $Li_2CuTlBr_6$, the value is 2.2 at 1.6 eV. These highest peaks are caused by the shift among Li-2s to Cl/Br-p states within the conduction band (CB). Compared to other perovskites, $Li_2CuTlBr_6$ has a lower bandgap value and a greater peak value, making it simpler to polarise CB electrons and increasing the photovoltaic effects. Thus, the materials under analysis function best in visible areas, qualifying for optoelectronic applications.

Plotting α(ω) versus photon energy yields a graph that offers precise details on the material's light-absorbing ability. The lean absorption of a material with a broader bandgap within the visible spectrum confirms the inverse relationship between bandgap as well as absorption threshold. As can be observed in Figure 5(e), the materials under investigation have a small bandgap that results in effective absorption in the visible spectrum. For DPs $Li_2CuTlCl_6$ and $Li_2CuTlBr_6$, the calculated absorption edges are 0.8 eV and 0.4 eV, correspondingly. The first peak absorption coefficient in both DPs in the IR light spectrum is measured at 2 eV and is 14×10^4 cm^{-1}. This is attributed to the transitions from Li-2s to Cl/Br-p. Referring to Fig. 5(e); maximum absorption coefficients within the visible range for $Li_2CuTlCl_6$ along with $Li_2CuTlBr_6$ are 16.2×10^4 cm^{-1} at 2.2 eV & 14.4×10^4 cm^{-1} during 1.9 eV, respectively. These measured absorption coefficients span the whole visible spectrum but remain quite high.

The curve patterns for $\varepsilon_1(\omega)$ with n(ω) seem nearly identical since comparable information is employed (refer to Figure 5(a and c)). For DPs $Li_2CuTlCl_6$ and $Li_2CuTlBr_6$, the estimated static refractive index, or n(0) is 1.9 and 2.2, respectively. Furthermore, the connection is supported by the static real dielectric constants of DPs $Li_2CuTlCl_6$ and $Li_2CuTlBr_6$, which are 3.4 and 4.4, respectively $n(\omega) = \sqrt{\epsilon_1(\omega)}$ [51].

The extinction coefficient, which corresponds to the compound's capacity to absorb radiations at a certain energy, is another essential physical characteristic. There are many peaks in the extinction coefficients associated with transitions from unfilled states in the conduction band and filled states in the valence band (see Fig. 5c). There is a relationship between the absorption coefficients and the imaginary dielectric constant and the extinction coefficients [52]. An analogous pattern is shown by α(ω), $\varepsilon_2(\omega)$ and extinction coefficients. The ability of a substance to reflect incoming energy over its surface is measured by its reflectivity. The measured static reflectance R(0) for DPs $Li_2CuTlCl_6$ and $Li_2CuTlBr_6$ is shown in Fig. 5(f) as 9% and 14%, respectively. The decrease in incoming energy absorption is the cause of the rise in reflectance.

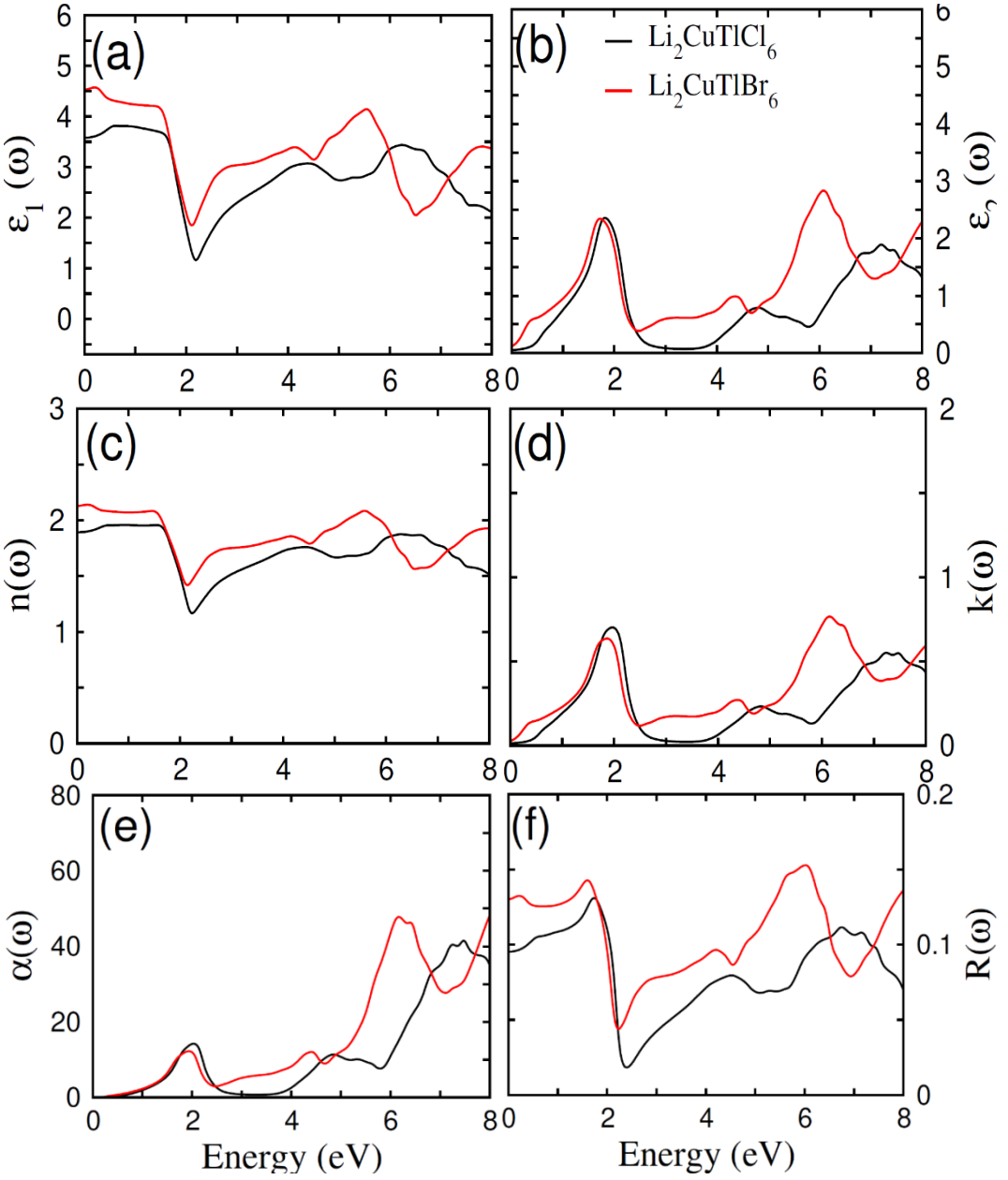

Fig. 5. The computed (a) real part $\varepsilon_1(\omega)$, (b) imaginary part $\varepsilon_1(\omega)$, (c) refractive index $n(\omega)$, (d) the extinction co-efficient $k(\omega)$, (e) absorption $\alpha(\omega)$, (f) reflectivity $R(\omega)$ of $Li_2CuTlCl_6$ and $Li_2CuTlBr_6$ halides.

3.4. Thermal Characteristics

Owing to the need to recycle and produce energy from renewable resources, temperature gradients that produce electrical energy utilizing thermoelectric materials are essential. Therefore, while constructing devices, the thermal characteristics of DPs $Li_2CuTlCl_6$ and $Li_2CuTlBr_6$ play a vital role. One well-known computational method for assessing a material's transport behavior over a wide range of frequencies utilizes the BoltzTraP code. Considering the temp domain (200-800 K), the thermoelectric efficiencies of DPs $Li_2CuTlCl_6$ and $Li_2CuTlBr_6$ are fully assessed, taking into account factors; power factor, Seebeck coefficient, ZT value, Cv value as well as respective conductivities.

As the temperature rises, charge carriers in semiconductors jump from VB to CB with enough energy. Up to 800 K, a steady rise in electrical conductivity has been observed. As seen in Figure 6a, $Li_2CuTlCl_6$ exhibits a faster increase in electrical conductivity than Li_2KTlBr_6. As shown in Figure 6c, the studied compounds thermal conductivity also increased to a maximum of

800K. The temperature-dependent ratio of thermal conductivity to electrical conductivity may be used to determine favorable transport behavior in a material and identify prospective applications in thermoelectric devices by using the Weidman-Franz equation (LT=κ/σ). The evaluated materials are qualified for thermoelectric use as they satisfy the requirements.

The materials used during investigations of the Seebeck coefficient (S) are displayed in Figure 6b. Both of the studied materials Seebeck coefficients show divergence above 800K, compared to the previous convergence noted in S as high as 200K. Because of the positive Seebeck coefficient (S) values, both materials under study have p-type characteristics.

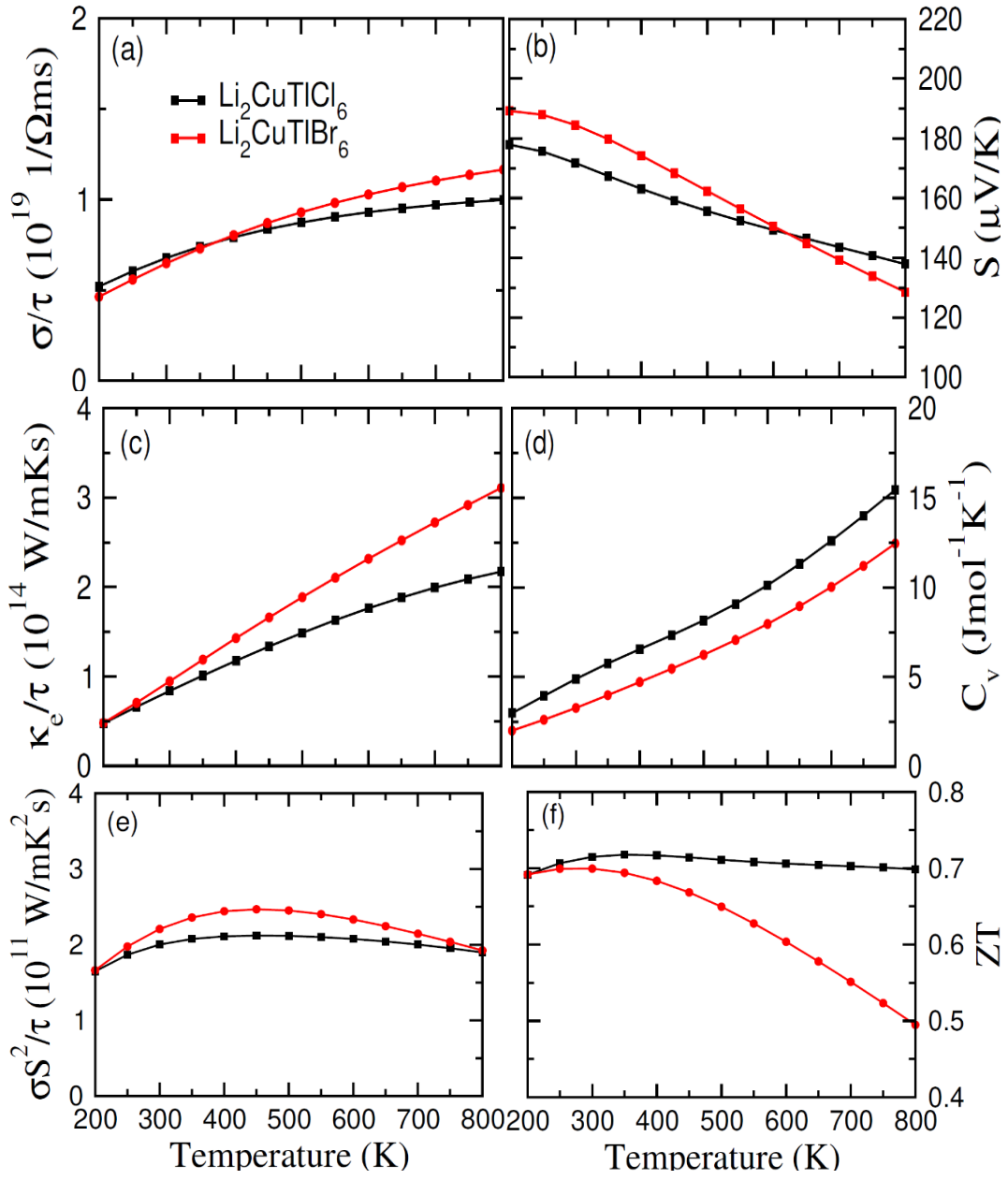

Fig. 6. The estimated (a) electrical conductivity (σ/τ), (b) Seebeck coefficients (S), (c) thermal conductivity (k_e/τ), (d) Specific heat capacity (Cv), (e) power factor and (f) figure of merit against the temperature of $Li_2CuTlCl_6$ and $Li_2CuTlBr_6$ halides.

Furthermore, studies on heat capacity (Cv), the percentage of the specimen's total heat energy to the induced thermal gradient, have been carried out between 200 and 800 K in temperature. As the temperature rises, both of the double perovskites heat capacities (Cv) increase (see Fig. 6d). For DPs $Li_2CuTlCl_6$ and $Li_2CuTlBr_6$, the reported ambient temp values of Cv have 5 J/mol-K and 3 J/mol-K, accordingly. One important component that must be considered when assessing the material's thermal efficiency is the power factor or rating. The power factor values for both double perovskites grow to 800K, as shown in Figure 6f. Both double perovskites show a comparable rising tendency within the given temperature range. However, $Li_2CuTlCl_6$ continues to have a slightly higher value than $Li_2CuTlCl_6$. The material's efficiency was assessed via the formula $ZT=(\sigma S^2/\kappa)T$, here, T illustrates the temperature in absolute terms. Higher Seebeck coefficients and optical conductivity must be used for a better ZT, and thermal conductivity must be kept to a minimum. [53]. As shown in Figure 6f, the estimated ZT values at room temperature are 0.72 for $Li_2CuTlCl_6$ and 0.70 for $Li_2CuTlBr_6$. These findings suggest that the two double perovskites under analysis are suitable for application in thermal-based appliances.

4. Conclusion

The mechanical characteristics of the DPs Li_2CuTlZ_6 (Z = Cl, Br, I) were investigated via DFT-oriented Wien2k and BoltzTraP initiatives. All materials show -ve E_{Form} and computed elastic constants, suggesting that the materials are dynamic as well as stable in structure within the cubic phase. Additionally, the positive values of elastic constants support their overall structural robustness by indicating their mechanical stability. The Poisson's ratio for $Li_2CuTlBr_6$ is 0.38, but it rises to 0.37 for $Li_2CuTlCl_6$. According to the study, all double perovskites are highly ductile, as shown by their Pugh's ratio, which varies between 3.27 and 3.04 eV. Furthermore, the band structure analysis shows the direct bandgap of studied DPs, suggesting potential applications in optoelectronics technology. These DPs maximum optical absorption properties in the IR region suggest that optoelectronic uses and optoelectronic devices are suitable for use. These materials appear well suited for thermoelectric applications based on their ZT value of approximately unity.

Funding

Researchers supporting project number (RSPD2024R741), King Saud University.

Acknowledgments

The authors would like to thank the Researchers Supporting Project number (RSPD2024R741), King Saud University, Riyadh, Saudi Arabia.

References

[1] A. Kojima, K. Teshima, Y. Shirai, T. Miyasaka, J. Am. Chem. Soc. 131 (2009) 6050-6051; https://doi.org/10.1021/ja809598r

[2] Y. Shao, Y. Yuan, J. Huang, Nat. Energy 1 (2016) 1-6; https://doi.org/10.1038/nenergy.2015.1

[3] S.S. Shin, E.J. Yeom, W.S. Yang, S. Hur, M.G. Kim, J. Im, J. Seo, J.H. Noh, SI Seok, Science 356 (2017) 167-171; https://doi.org/10.1126/science.aam6620

[4] M.M. Lee, J. Teuscher, T. Miyasaka, T.N. Murakami, H.J. Snaith, Science 338 (2012) 643-647; https://doi.org/10.1126/science.1228604

[5] G.-H. Kim, D.S. Kim, Joule 5 (2021) 1033-1035; https://doi.org/10.1016/j.joule.2021.04.008

[6] J. Jebakumar, D.J. Moni, D. Gracia, M.D. Shallet, Appl. Nanosci. (2022) 1-12;

https://doi.org/10.1007/s13204-021-02268-7
[7] F. Igbari, Z.K. Wang, L.S. Liao, Adv. Energy Mater. 9 (2019), 1803150; https://doi.org/10.1002/aenm.201803150
[8] S.E. Creutz, E.N. Crites, M.C. De Siena, D.R. Gamelin, Nano Lett. 18 (2018) 1118-1123; https://doi.org/10.1021/acs.nanolett.7b04659
[9] C.J. Bartel, J.M. Clary, C. Sutton, D. Vigil-Fowler, B.R. Goldsmith, A.M. Holder, C. B. J. Am. Chem. Soc. 142 (2020) 5135-5145; https://doi.org/10.1021/jacs.9b12440
[10] A. Jain, O. Voznyy, E.H. Sargent, J. Phys. Chem. C 121 (2017) 7183-7187; https://doi.org/10.1021/acs.jpcc.7b02221
[11] S.Y. Liu, M. Sun, S. Zhang, S. Liu, D.J. Li, Z. Niu, Y. Li, S. Wang, Appl. Phys. Lett. 118 (2021) 141903; https://doi.org/10.1063/5.0043809
[12] S. Zelewski, J. Urban, A. Surrente, D. Maude, A. Kuc, L. Schade, R. Johnson, M. Dollmann, P. Nayak, H. Snaith, J. Mater. Chem. C 7 (2019) 8350-8356; https://doi.org/10.1039/C9TC02402F
[13] W. Shi, T. Cai, Z. Wang, O. Chen, J. Chem. Phys. 153 (2020), 141101; https://doi.org/10.1063/5.0021238
[14] S. Zhao, K. Yamamoto, S. Iikubo, S. Hayase, T. Ma, J. Phys. Chem. Solid. 117 (2018) 117-121; https://doi.org/10.1016/j.jpcs.2018.02.032
[15] W. Zhou, P. Han, X. Zhang, D. Zheng, S. Yang, Y. Yang, C. Luo, B. Yang, F. Hong, D. Wei, J. Phys. Chem. Lett. 11 (2020) 6463-6467; https://doi.org/10.1021/acs.jpclett.0c01968
[16] X.-G. Zhao, J.-H. Yang, Y. Fu, D. Yang, Q. Xu, L. Yu, S.-H. Wei, L. Zhang, J. Am. Chem. Soc. 139 (2017) 2630-2638; https://doi.org/10.1021/jacs.6b09645
[17] H.-J. Feng, W. Deng, K. Yang, J. Huang, X.C. Zeng, J. Phys. Chem. C 121 (2017) 4471-4480; https://doi.org/10.1021/acs.jpcc.7b00138
[18] A.M. Jafar, K.A. Khalaph, A.M. Hmood, IOP Publishing, 2020, 012047; https://doi.org/10.1088/1757-899X/765/1/012047
[19] X. Chen, C. Wang, Z. Li, Z. Hou, W.-J. Yin, Sci. China Mater. 63 (2020) 1024-1035; https://doi.org/10.1007/s40843-019-1255-4
[20] M. Roknuzzaman, C. Zhang, K.K. Ostrikov, A. Du, H. Wang, L. Wang, T. Tesfamichael, Sci. Rep. 9 (2019) 1-7; https://doi.org/10.1038/s41598-018-37132-2
[21] E. Meyer, D. Mutukwa, N. Zingwe, R. Taziwa, Metals 8 (2018) 667; https://doi.org/10.3390/met8090667
[22] G. Volonakis, M.R. Filip, A.A. Haghighirad, N. Sakai, B. Wenger, H.J. Snaith, F. Giustino, J. Phys. Chem. Lett. 7 (2016) 1254-1259; https://doi.org/10.1021/acs.jpclett.6b00376
[23] T.M. Bhat, D.C. Gupta, J. Phys. Chem. Solid. 112 (2018) 190-199; https://doi.org/10.1016/j.jpcs.2017.09.023
[24] H. Huang, X. Fan, D.J. Singh, W. Zheng, J. Mater. Chem. C 8 (2020) 9763-9774; https://doi.org/10.1039/D0TC01488E
[25] R. Singh, R. Kottokkaran, V.L. Dalal, G. Balasubramanian, Nanoscale 9 (2017) 8600-8607; https://doi.org/10.1039/C7NR00459A
[26] L. Yu, W. Kassem, R. Bude, L. Divay, J. Amrit, S. Volz, IEEE, 2015, pp. 1-5.
[27]. N. Guechi, A. Bouhemadou, S. Bin-Omran, A. Bourzami, L. Louail, J. Electron. Mater. 47 (2018) 1533-1545; https://doi.org/10.1007/s11664-017-5962-2
[28] D. Behera, Batouche Mohammed, Seddik Taieb, Boudjelal Mokhtar, Samah Al-Qaisi, Sanat Kumar Mukherjee, The European Physical Journal Plus 138 (2023) 520; https://doi.org/10.1140/epjp/s13360-023-04137-4
[29] M. Caid, D. Rached, S. Al-Qaisi, Y. Rached, H. Rached. Solid State Commun. 369 (2023) 115216; https://doi.org/10.1016/j.ssc.2023.115216
[30] K. Schwarz, P. Blaha, G.K. Madsen, Comput. Phys. Commun. 147 (2002) 71-76; https://doi.org/10.1016/S0010-4655(02)00206-0
[31] J.P. Perdew, K. Burke, M. Ernzerhof, Phys. Rev. Lett. 77 (1996) 3865;

https://doi.org/10.1103/PhysRevLett.77.3865
[32]. F. Tran, P. Blaha, Phys. Rev. Lett. 102 (2009), 226401; https://doi.org/10.1103/PhysRevLett.102.226401
[33] G.K. Madsen, D.J. Singh, Boltz TraP., Comput. Phys. Commun. 175 (2006) 67-71; https://doi.org/10.1016/j.cpc.2006.03.007
[34] S. Al-Qaisi, D. Rai, B.U. Haq, R. Ahmed, T.V. Vu, M. Khuili, S.A. Tahir, H. H. Alhashim, Mater. Chem. Phys. 258 (2021), 123945; https://doi.org/10.1016/j.matchemphys.2020.123945
[35] Y. Rached, M. Caid, H. Rached, M. Merabet, S. Benalia, S. Al-Qaisi, L. Djoudi, D. Rached, J. Supercond. Nov. Magnetism 35 (2022) 875-887; https://doi.org/10.1007/s10948-021-06131-2
[36] S.I. Ranganathan, M. Ostoja-Starzewski, Phys. Rev. Lett. 101 (2008), 055504; https://doi.org/10.1103/PhysRevLett.101.055504
[37] X. Luan, H. Qin, F. Liu, Z. Dai, Y. Yi, Q. Li, Crystals 8 (2018) 307; https://doi.org/10.3390/cryst8080307
[38] B. Huang, Y.-H. Duan, W.-C. Hu, Y. Sun, S. Chen, Ceram. Int. 41 (2015) 6831-6843; https://doi.org/10.1016/j.ceramint.2015.01.132
[39] J.-M. Zhang, Y. Zhang, K.-W. Xu, V. Ji, J. Phys. Chem. Solid. 68 (2007) 503-510; https://doi.org/10.1016/j.jpcs.2007.01.025
[40] P. Wachter, M. Filzmoser, J. Rebizant, Phys. B Condens. Matter 293 (2001) 199-223; https://doi.org/10.1016/S0921-4526(00)00575-5
[41] R. Hill, Proc. Phys. Soc. 65 (1952) 349; https://doi.org/10.1088/0370-1298/65/5/307
[42] S. Pugh, Dublin Phil. Mag. J. Sci. 45 (1954) 823-843; https://doi.org/10.1080/14786440808520496
[43] F. Elfatouaki, O. Farkad, E. Ibnouelghazi, D. Abouelaoualim, A. Outzourhit, Mater. Sci. Semicond. Process. 143 (2022), 106488; https://doi.org/10.1016/j.mssp.2022.106488
[44]. K. Khan, J. Sahariya, A. Soni, Mater. Chem. Phys. 262 (2021), 124284; https://doi.org/10.1016/j.matchemphys.2021.124284
[45] G. Remil, A. Zitouni, B. Bouadjemi, M. Houari, A. Abbad, W. Benstaali, S. Cherid, M. Matougui, T. Lantri, S. Bentata, Solid State Commun. 336 (2021), 114422; https://doi.org/10.1016/j.ssc.2021.114422
[46] C. Ambrosch-Draxl, J.O. Sofo, Comput. Phys. Commun. 175 (2006) 1-14; https://doi.org/10.1016/j.cpc.2006.03.005
[47] P.K. Kamlesh, R. Gautam, S. Kumari, A.S. Verma, Phys. B Condens. Matter (2020), 412536; https://doi.org/10.1016/j.physb.2020.412536
[48] BU. Haq, S. AlFaify, T.A. Alrebdi, R. Ahmed, S. Al-Qaisi, M. Taib, G. Naz, S. Zahra, Mater. Sci. Eng., B 265 (2021), 115043; https://doi.org/10.1016/j.mseb.2021.115043
[49] M. Ezzeldien, S. Al-Qaisi, Z. Alrowaili, M. Alzaid, E. Maskar, A. Es-Smairi, T.V. Vu, D. Rai, Sci. Rep. 11 (2021) 1-12; https://doi.org/10.1038/s41598-021-99551-y
[50]. E. Maskar, A.F. Lamrani, M. Belaiche, A. Es-Smairi, M. Khuili, S. Al-Qaisi, T.V. Vu, D. Rai, Surface. Interfac. 24 (2021), 101051; https://doi.org/10.1016/j.surfin.2021.101051
[51]. D. Rai, A. Laref, M. Khuili, S. Al-Qaisi, T.V. Vu, D.D. Vo, Vacuum 182 (2020), 109597; https://doi.org/10.1016/j.vacuum.2020.109597
[52] M. Fox, American Association of Physics Teachers, 2002; https://doi.org/10.1119/1.1691372
[53] O. Hellman, D.A. Broido, Phys. Rev. B 90 (2014), 134309; https://doi.org/10.1103/PhysRevB.90.179904